

Synthesis and Characterization of Nickel Doped Iron Oxide Nano Particles

Abbas Adeel¹, Arshad Javid Muhammad¹, Ahtisham Anjum², Sardar Sikandar Hayat³, Muhammad Sultan¹

¹ Department of Basic Sciences, University of Engineering & Technology, Taxila, Pakistan .47050

¹ MS Scholar , Department of Basic Sciences, University of Engineering & Technology, Taxila, Pakistan.47050;

² Functional materials Lab, Department of Physics, Air University, PAF Complex E-9, Islamabad. Pakistan.

³ Department of Physics, Faculty of Basic and Applied Sciences, International Islamic University Chitral, H-10, Islamabad, Pakistan

* Correspondence: Dr. Muhammad Arshad Javid, Department of Basic Sciences, University of Engineering & Technology, Taxila, Pakistan .47050

Abstract

The objective of this work is to synthesize and characterize nickel ferrite to improve the magnetic saturation. For structural analysis, XRD was revealed that Ni-doped Fe_2O_3 have a cubic spinel structure. From XRD data, the grain size of $NiFe_2O_4$ was observed to be (17.12 nm) after 20 wt.% Ni-doped Fe_2O_3 , and its further increases up to 19.36 nm for 40 wt.% $NiFe_2O_4$, respectively. The XRD pattern confirmed that doping of Ni metal increased the grain size of nanoparticles. SEM was performed to study the morphology of prepared samples. EDX was performed to confirm the elemental analysis. Saturation magnetization (M_s) was improved with concentration of dopant material Ni (20 wt.%, 40 wt.%) in magnetic nanoparticles. In conclusion, this study demonstrates the very easy way of synthesis of Ni doped iron oxides nanoparticles for magnetic material applications

Keywords: Nickel ferrites; Magnetic nanoparticles; VSM, Magnetic saturation

Date of Submission: 17-10-2021

Date of acceptance: 01-11-2021

I. Introduction

Magnetic nanoparticles were significantly studied for biomedical research such as drug delivery, hyperthermia in cancer, protein separation, biosensing and magnetic resonance imaging (MRI) [1, 2], [3]. Since the late 1990s, iron oxide-based nanoparticle contrast agents have been explored and clinically used as T2-weighted contrast agents. They compose magnetic nanoparticle core and biocompatible coating material, preventing aggregation and sedimentation and allowing high biological tolerance [4]. Recently, researchers have focused on nickel ferrite nanoparticles as MRI contrast agents due to their high magnetic susceptibility, biocompatibility, biodegradability and nontoxicity characteristics [5]. Several studies have investigated the nickel-based nanoparticles as an alternative to gadolinium for reducing the risk of toxicity [6]. Nickel metal also possesses a high spin quantum number and proton exchange kinetics [7]. MRI has several blessings over unique imaging modalities due to excessive spatial selection, amazing clean tissue evaluation and non-utilization of radioisotopes. Paramagnetic gadolinium complexes are commonly used as MRI contrast agent [8]. However, gadolinium-based complexes have low sensitivity and have toxic outcomes that incorporate nephrogenic systemic fibrosis (NSF) [9].

In this research work, nickel doped iron oxide nanoparticle have been synthesized using co-precipitation method to enhance the saturation magnetization of magnetic nanoparticles.

II. Experimental

Ferric chloride hexahydrate ($FeCl_3 \cdot H_2O$), ferrous chloride tetra-hydrate ($FeCl_2 \cdot H_2O$), nickel chloride hexahydrate ($NiCl_2 \cdot H_2O$) and ammonium hydroxide (NH_4OH) were used for the preparation of Fe_3O_4 and $NiFe_2O_4$ superparamagnetic nanoparticles using co-precipitation method. Distilled water was used as a solvent to remove the impurities in the final product. [3]. First, the solution of $NiCl_2 \cdot 6H_2O$ was prepared in distilled water and stirred for 1 hour at 50°C approximately. Then the solution of $FeCl_2 \cdot 4H_2O$ was prepared in the distilled water and stirred for 1 hour at 50°C. Then solutions of $NiCl_2 \cdot 6H_2O$ and $FeCl_2 \cdot 4H_2O$ were mixed

with continuous stirring at 60 °C. Then NaOH was added drop wise upto pH 10. Oleic acids were added in the same solution as a capping agent and surfactant. The precipitation was washed out with distilled water and dried in the oven at 60 °C for 8 hours.

III. Results and Discussion

3.1. XRD analysis

XRD pattern for Ni-doped iron oxide $Ni_{0.2}Fe_{2.8}O_4$ and $Ni_{0.4}Fe_{2.6}O_4$ was shown in Figure 1. Diffracting peaks of all prepared samples were depicted in Figure 1 at $2\theta = 29.94^\circ, 35.57^\circ, 37.13^\circ, 43.32^\circ, 47.33^\circ, 54.11^\circ, 57.21^\circ$ and 62.95° with miller indices (220), (311), (222), (400), (331), (422), (333), and (440) respectively.

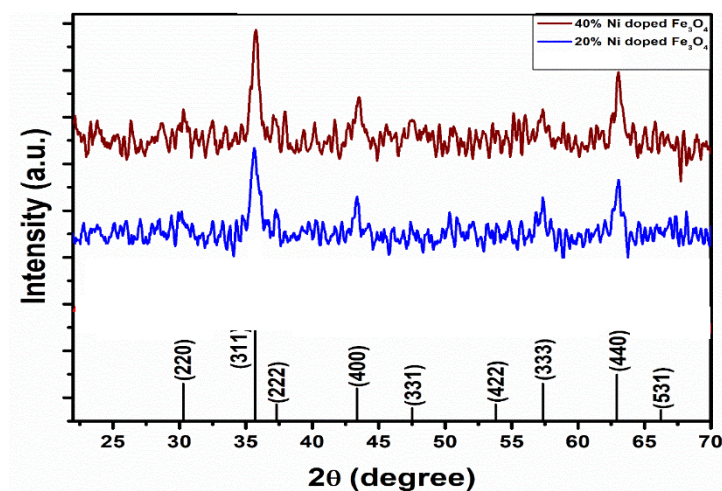


Figure 1. XRD pattern of $NiFe_2O_4$.

The XRD diffraction peaks of the $Ni_{0.2}Fe_{2.8}O_4$ (S_2), and $Ni_{0.4}Fe_{2.6}O_4$ (S_3), belongs to the FCC structure, which can be well-matched with (JCPDS) card no (00-010-0325). Diffraction peaks and their sharpness define the degree of crystallinity. There are no other extra secondary phases, suggesting that the ions of Ni^{2+} are entirely diffused into the A-site which is Fe^{2+} in Fe_3O_4 . For the calculation of the lattice parameter following relation was used:

$$a = d_{hkl}(\sqrt{h^2 + k^2 + l^2}) \quad (1)$$

$$n\lambda = 2d \sin\theta \quad (2)$$

For the calculation of crystallite size following equation was used:

$$D = \frac{K \times \lambda}{\beta \times \cos\theta} \quad (3)$$

Where D represents the crystallite size of the diffraction peak, K represents the shape factor of the particles which is 0.9, λ is the wavelength of the radiation has the value 1.54 \AA , β is the full width at half maxima of the diffraction peak, and θ is the corresponding Bragg's diffraction angle.

Table 1. Average grain size $NiFe_2O_4$

Sr. No	Material	Grain Size (nm)
2	$Ni-Fe_2O_4$ (20% wt)	17.12
3	$Ni-Fe_2O_4$ (40% wt)	19.36

3.2. SEM analysis

The surface morphology of Ni-doped Fe_2O_4 was studied through SEM model Instrument JSM-5910, Japan at 20.0 kV. SEM confirmed that particles are spherical in shape and most of them are in flask shape [10]. The density of the particles was also increased with the increase in the concentration of Ni in Fe.

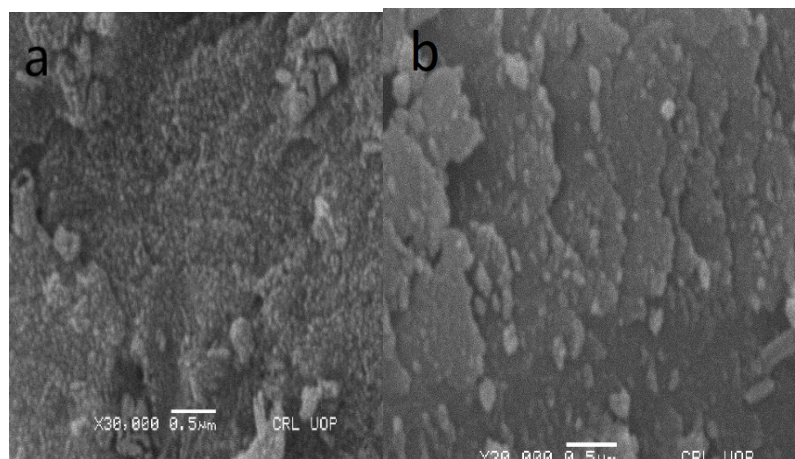


Figure 2. SEM of Ni-doped Fe_3O_4 (a) 20% Ni – doped Fe_2O_4 and (b) 40% Ni – doped Fe_2O_4

3.3. Vibrating Sample Magnetometer (VSM)

Magnetic properties of prepared samples such as saturation magnetization were measured at room temperature using Deking Magnet Tech Co, Model (VSM-100), China. Ni-doped Fe_2O_4 nanoparticles did not depicted hysteresis curve. This saturation magnetization confirmed that all the samples have superparamagnetic behavior in nature. The magnetization curve showed high saturation magnetization and low coercive force. The saturation magnetization was increased from 48.96 emu/cm^3 to 126.7 emu/cm^3 . The total magnetic moment of the system is increased and therefore the magnetization of the system also increases. There is no detectable change observed in coercive field values that are 0.0094 and 0.0095 T for 20% Ni-doped Ni and 40% Ni-doped ferrite, respectively.

Where H_c represents the coercive field and M_s shows saturation magnetization, while anisotropy constant value K depends upon the concentration of dopant material. It means that the anisotropy constant of the system increases with the increasing content of Ni.

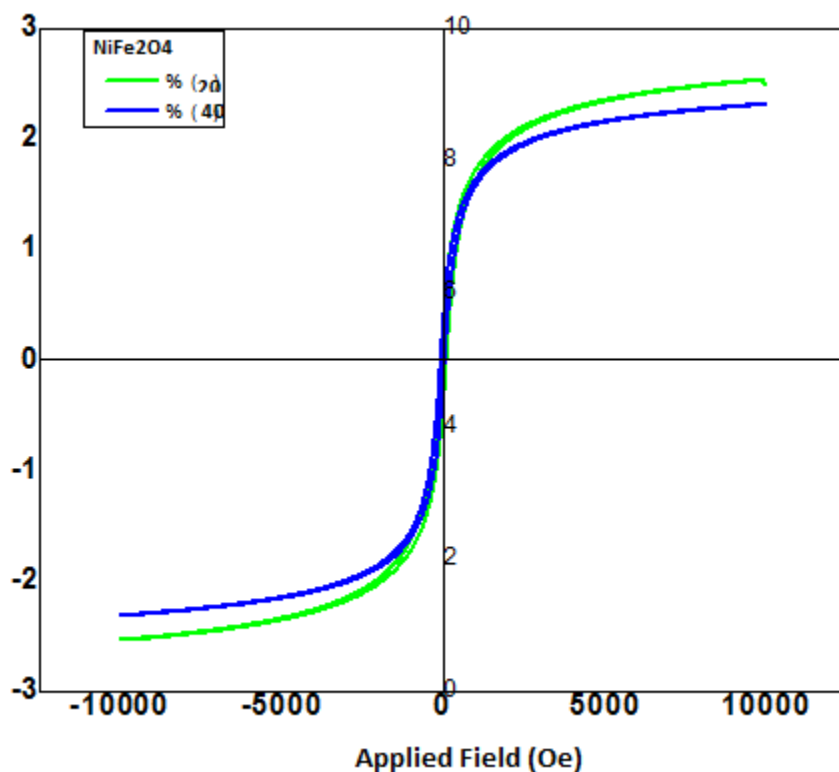


Figure 3. M-H loop for Ni-doped Fe_2O_4

IV. Conclusions

In this study, Ni-doped iron oxides nanoparticles were prepared using co-precipitation method at room temperature. The structural conformation was done with XRD which exhibit spinal cubic structure of magnetic nanoparticles. The surface morphology of samples revealed that particles depicted the flat surface and have negligible agglomeration in SEM analysis. The saturation magnetization for NiFe₂O₄ was enhanced 115.55, to 126.7 emu/cm³ after Ni doping with 20wt. % and 40 wt. % Ni, respectively. Therefore, this study concludes that nickel ferrites may be used in magnetic technology to enhance its magnetic saturation.

Funding

“This research received no external funding”

Conflicts of Interest

Declare conflicts of interest or state “The authors declare no conflict of interest.”

References

- [1]. Bai, C., et al., Synthesis of Ultrasmall Fe₃O₄ Nanoparticles as T₁-T₂ Dual-Modal Magnetic Resonance Imaging Contrast Agents in Rabbit Hepatic Tumors. *ACS Applied Nano Materials*, 2020. **3**(4): p. 3585-3595.
- [2]. Vangijzegem, T., et al., Influence of experimental parameters of a continuous flow process on the properties of very small iron oxide nanoparticles (VSION) designed for T₁-weighted magnetic resonance imaging (MRI). *Nanomaterials*, 2020. **10**(4): p. 757.
- [3]. Thomsen, H.S., Nephrogenic systemic fibrosis and gadolinium-based contrast media, in *Contrast Media*. 2014, Springer. p. 207-217.
- [4]. Senpan, A., et al., Conquering the dark side: colloidal iron oxide nanoparticles. *Acs Nano*, 2009. **3**(12): p. 3917-3926.
- [5]. Vuong, Q.L., et al., A universal scaling law to predict the efficiency of magnetic nanoparticles as MRI T₂-contrast agents. *Advanced healthcare materials*, 2012. **1**(4): p. 502-512.
- [6]. Ward, K., A. Aletras, and R.S. Balaban, A new class of contrast agents for MRI based on proton chemical exchange dependent saturation transfer (CEST). *Journal of magnetic resonance*, 2000. **143**(1): p. 79-87.
- [7]. Dula, A.N., S.A. Smith, and J.C. Gore, Application of chemical exchange saturation transfer (CEST) MRI for endogenous contrast at 7 Tesla. *Journal of Neuroimaging*, 2013. **23**(4): p. 526-532.
- [8]. Mao, Z., et al., A positively charged small-molecule T₁ magnetic resonance imaging contrast agent for highly efficient labeling and tracking adipose tissue-derived stem cells. *Materials Today Communications*, 2020. **25**: p. 101627.
- [9]. Maheshwaran, D., et al., Smart dual T₁ MRI-optical imaging agent based on a rhodamine appended Fe (iii)-catecholate complex. *Dalton Transactions*, 2020. **49**(41): p. 14680-14689.
- [10]. Hu, P., et al., High saturation magnetization Fe₃O₄ nanoparticles prepared by one-step reduction method in autoclave. *Journal of Alloys and Compounds*, 2017. **728**: p. 88-92.